Evaluating image analysis techniques for ultrasound optical tomography in breast tissue

Henrik von Friesendorff

2023

LUND
UNIVERSITY

Supervisor: Stefan Kröll
Assistant supervisor: David Hill
Examiner: Magnus Cinthio

Master's Thesis in Biomedical Engineering
Department of Atomic Physics
Department of Biomedical Engineering
Faculty of Engineering, LTH

Abstract

Breast cancer is the most commonly diagnosed cancer in the world today and early detection is crucial to minimize the mortality. "Ultrasound optical tomography" (UOT) is a method under development for deep tissue imaging. The technique combines the resolution of ultrasound with the tissue contrast from light to image optical absorption in tissues. This report presents simulations analyzing how changing the light configuration can improve the imaging performance as well as two reconstruction methods, relative and absolute absorption reconstruction, to process the signal to be able to detect tumors. The simulations were conducted using a simulated breast tissue sample with *in vivo* optical parameters. The results indicated that a larger light-source can increase the power and improve the signal-to-noise ratio and contrast-to-noise ratio. Both reconstruction methods improved the readability compared to the raw signal. The ratio reconstruction performed well in localizing the tumor but with poor resolution while the absorption reconstruction revealed the tumor with high resolution and contrast but the method also generated artifacts. In conclusion, indications suggest that a larger light-source will improve the performance of a UOT-system and the two reconstructions method can enhance the detection capability of the signal but neither has a high enough performance to work on its own at this stage and further developments are required.

Populärvetenskaplig sammanfattning

Analys av Ultraljuds Optisk Tomografi som bildtagningsmetod

Bröstcancer är den idag vanligaste cancerformen och drabbar varje år fler än 2 miljoner kvinnor världen över. Chansen att överleva har ökat mycket de senaste årtiondena, mycket tack vare screening och tidig behandling, men fortfarande överlever inte var tionde drabbad i Sverige. En ny teknik för att i ett tidigt stadie kunna upptäcka små tumörer, som inte går att se med vanlig röntgen eller ultraljud, är "Ultrasound optical tomography" (UOT) som kombinerar ultraljud med laser för att kunna se små vävnadsförändringar inne i kroppen. Det är fortfarande några år innan tekniken är redo att börja användas på människor men man har gjort försök på vävnadsprover som ska efterlikna mänsklig vävnad och sett lovande resultat.

Att genomföra experiment kräver mycket tid och resurser och för att veta vilka experiment som bör utföras använder sig ofta forskare av simuleringsverktyg. I det här arbetet genomfördes simuleringar för att efterlikna komplexiteten av de olika vävnadstyper som finns inne i ett bröst. Undersökningar av hur bildtagningen med UOT kan utformas för att ge så bra bilder som möjligt utfördes också.

Den första delen av simuleringarna fokuserade på hur det inkommande ljuset ska distribueras för ge så mycket och tydlig signal som möjligt. Resultaten visade bland annat att en laser som sprider ljuset över en stor yta, och gör att man kan skicka in mer ljus på en gång, leder till att bilderna får mindre brus och att man får större möjlighet att skilja tumörerna från vanlig bröstvävnad.

Den andra delen av arbetet fokuserade på att utvärdera olika verktyg som kan användas när signalen från UOT-systemet analyseras. I den "råa" signalen som uppmäts vid en bildtagning är det nästan omöjligt att med blotta ögat se vad bilderna föreställer. Därför testades två matematiska metoder för att förtydliga bildinnehållet. Den första metoden var att jämföra signalen från en bild på en tumör med signalen från en bild på vanlig bröstvävnad och dividera dessa signaler med varandra. På så sätt kan man framhäva skillnaderna och se var det finns intressanta områden i bilden med tumören. Metoden visade sig vara bra på att hitta tumören men den var inte så bra på att bestämma storleken på den. Den andra metoden innebar också att jämföra signalen från bilden på tumören med signalen från en bild på bröstvävnad. I det här fallet testar man istället att lägga till en tumör i bilden på vanlig bröstvävnad och ser vad som händer med signalen. Genom att testa för flera digitala tumörer med olika placeringar

så får man till slut en signal som liknar den från tumörbilden och då vet man var tumören fanns i originalbilden. Den här metoden var bra på att hitta och placera ut tumören men resultatet angav också att det fanns fler tumörer än som fanns i originalbilden.

Bröstcancer är trots pågående framsteg fortfarande ett stort problem, men UOT har potential att bli ett effektivt framtida verktyg för detektering av mindre tumörer. Detta examensarbete har visat några potentiella utvecklingsområden men också lyft några utmaningar som kommer med dessa lösningar.

Acknowledgments

First of all I would like to thank my supervisor Stefan Kröll for all the interesting insights and discussions throughout the project.

I would also like to thank my assistant supervisor David Hill for all explanations, encouragement and attempting to teach me all worth knowing about lasers, rare-earth-ion-doped crystals and quantum mechanics.

A big thank you to Predrag Bakic and Sophia Zackrisson for providing the breast tissue phantoms and relevant clinical aspects.

Contents

Abstract **I**

Populärvetenskaplig sammanfattning **III**

Acknowledgments **V**

Abbreviations **IX**

1 Introduction **1**
1.1 Background . . . 1
1.2 Aim . . . 1

2 Background **3**
2.1 Light propagation . . . 3
2.1.1 Light in tissue . . . 3
2.1.2 Absorption in tissue . . . 4
2.1.3 Scattering in tissue . . . 5
2.2 Light-sound interaction . . . 5
2.3 Ultrasound optical tomography . . . 6
2.3.1 Light-tagging . . . 6
2.3.2 Rear-earth-ion-doped filters . . . 6
2.3.3 Medical safety limits . . . 8
2.4 Simulation tool . . . 9
2.4.1 Monte Carlo Simulation . . . 9
2.4.2 UOT-simulation . . . 9
2.4.3 Absorption reconstruction . . . 10

3 Methods **13**
3.1 Breast tissue phantoms . . . 13
3.1.1 Optical parameters . . . 13
3.1.2 Pre-processing . . . 14
3.2 Simulation set-up . . . 15
3.2.1 Transmission geometry . . . 15
3.2.2 Light configuration . . . 16
3.2.3 Light intensity . . . 17
3.2.4 Used parameters . . . 17
3.3 Light distribution analysis . . . 18
3.4 Image reconstruction analysis . . . 19

3.4.1 Ratio reconstruction 20
3.4.2 Absorption reconstruction 20

4 Results **21**
4.1 Tissue images 21
4.2 Light distribution analysis 21
4.2.1 SNR and CNR 23
4.3 Image reconstruction analysis 24
4.3.1 Ratio reconstruction 26
4.3.2 Absorption reconstruction 27

5 Discussion **29**
5.1 Optical parameters 29
5.2 Optical set-ups 29
5.2.1 Compared set-ups 29
5.2.2 Emitted photons 30
5.2.3 SNR and CNR comparison 30
5.3 Reconstructions 31
5.3.1 Ratio reconstruction 31
5.3.2 Absorption reconstruction 31
5.3.3 Future reconstruction improvements 32

6 Conclusion **35**

References **37**

List of abbreviations

CNR - Contrast-to-Noise Ratio
FFT - Fast Fourier Transform
Hb - Deoxygenated haemoglobin
HbO_2 - Oxygenated haemoglobin
MC - Monte Carlo
MCML - Monte Carlo model in multi-layered tissue
MPE - Maximum permissible exposure
PAT - Photo-acoustic tomography
SNR - Signal-to-Noise Ratio
UOT - Ultrasound optical tomography
US - Ultrasound

1 Introduction

1.1 Background

Breast cancer is the most commonly diagnosed cancer type in the world and also the type that causes most deaths among women [1]. The mortality has been reduced in the last decades and early detection and screening are believed to be contributing factors [2]. Small tumors can however be hard to detect in both mammography screening and through ultrasound imaging. "Ultrasound optical tomography" (UOT) is an imaging method under development that combines light and ultrasound to image differences in light absorption in biological tissue. The approach takes advantage of the contrast properties from light in tissue and the resolution from ultrasound and can therefore image differences more clearly than the two techniques separately. As the method presents more accurate results in tissue phantoms, the question of medical performance starts to actualize.

1.2 Aim

Recently, experiments on inhomogeneous tissue phantoms, with optical parameters corresponding to human breast tissue, have been performed with promising results [3]. In this thesis, a more complex tissue model, taking the different tissues in the breast into consideration is presented. We also present how different light configurations affect the resulting image and techniques that can be used to improve the analysis and extraction of important signal content.

2 Background

2.1 Light propagation

To understand the principle of ultrasound optical tomography one must understand the underlying mechanics of light. Light often refers to the visible part of the electromagnetic radiation spectrum. Electromagnetic radiation spans a large frequency range and, in addition to light, also includes other types of radiation such as heat (infrared), radio waves and X-rays. The propagation of light can be seen as a wave, which means that it has a wavelength and frequency but also as particles, or photons. These photons can interact with the medium and their propagation is affected by absorption and/or scattering. When a photon is absorbed by a molecule, one of the electrons elevates to a higher energy state, and becomes excited. The excited condition generally has a short duration followed by relaxation, when the electron returns to its ground state. During relaxation, the excess energy is radiated as heat and/or as another photon. Scattering is when the photon changes its propagation path and can be done in two ways, elastic or inelastic. In the case of elastic scattering, or reflection, the frequency and energy is preserved, whereas in inelastic scattering there is some energy transformation in the interaction which leads to a shift in frequency [4].

2.1.1 Light in tissue

Human tissue is characterized as being highly scattering with a scattering probability 1000 times larger than the absorption probability for some wavelengths. The optical absorption is mostly affected by haemoglobin – a molecule in red blood cells which binds to oxygen – and water. The absorption of haemoglobin is high for low wavelengths (< 600 nm) and the absorption of water is increasing with longer wavelengths. This results in the absorption being relatively low in the visible red to near infrared spectrum (650-1350 nm), what is often referred to as the tissue optical window, which is optimal for deep tissue imaging. In this window, the absorption of oxygenated (HbO_2) and deoxygenated haemoglobin (Hb) is at its minimum and the absorption from water is still low. In Figure 2.1, the first tissue optical window between 650-950 nm is highlighted. In the literature, further windows are suggested for higher wavelengths [4, 5]. An example of where the absorption is used is in instruments measuring oxygen saturation. These instruments measure the difference in absorption, which they use to calculate the difference between oxygenated and deoxygenated haemoglobin.

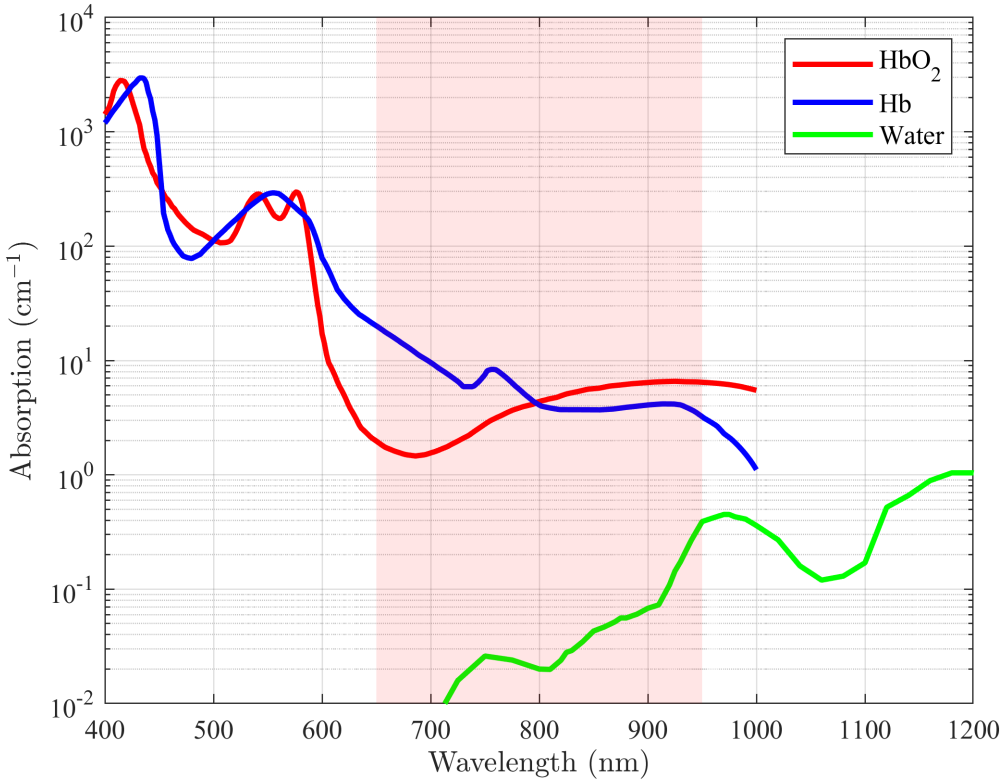

Figure 2.1: Diagram of the absorption coefficient of oxygenated haemoglobin (HbO_2), deoxygenated haemoglobin (Hb) and water for different wavelengths. The parameters are retrieved from Prahl [6]. The figure also highlights the first optical window between 650-950 nm, optimal for deep penetration depth. Note that the vertical axis is logarithmic.

2.1.2 Absorption in tissue

The absorption coefficient, μ_a, describes the mean unit path length before absorption and is defined as the probability of absorption per unit path length in a tissue type, or with the equation

$$\mu_a = -\frac{1}{I}\frac{dI(x)}{dx} \tag{2.1}$$

where $I(x)$ is the intensity of light at position x [4]. If the expression is integrated, I can further be described with the Beer-Lambert law

$$I(x) = I_0 e^{-\mu_a x} \tag{2.2}$$

which shows that the intensity of light when it has propagated a distance x, where I_0 is the intensity at point $x = 0$. If the relaxation does not lead to emission of a photon, we have so-called nonradiative relaxation, where energy is transformed into heat. Absorption in tissue is mainly affected by the concentration of haemoglobin and water [4].

2.1.3 Scattering in tissue

The scattering coefficient, μ_s, is defined as the probability of photon scattering per unit path length in a medium and is a combination of the scattering features of a single scatterer and its concentration in the medium [4]. The scattering properties are affected by the size of the structure and the photon wavelength, where the scattering effect is stronger for a wavelength that matches the biological structure size. The scattering in tissue can be simplified with Rayleigh theory which is when the particles are much smaller than the wavelength. Mie theory describes the scattering on spherical particles of all sizes. In tissue, the cell nuclei and mitochondria are the main scatterers.

The anisotropy, g, defined as $\langle \cos\theta \rangle$, describes the average forward component in the direction photons are scattered and g is given a value between -1 and 1. A value close to 1 indicates a forward scattering pattern and the value 0 is an isotropic scattering pattern. The relationship between the forward scattering angle θ and g is described by the Henyey-Greenstein phase function

$$p(\cos\theta) = \frac{1 - g^2}{2(1 + g^2 - 2\,g\cos\theta)^{3/2}} \tag{2.3}$$

which was initially used for scattering in interstellar dust clouds but is often used in describing scattering of light in tissue [7, 8]. The anisotropy in tissue is often $\sim$0.9 [4].

A commonly used simplification is using the reduced scattering coefficient

$$\mu_s' = \mu_s(1 - g). \tag{2.4}$$

Instead of following the entire path of the photon it describes an approximation of the photon position after a few scattering events. This variable is easier to obtain experimentally than μ_s and g [9].

2.2 Light-sound interaction

What is often referred to as sound is the propagation of a mechanical wave in air, liquid or a solid-state medium with a frequency that can be heard by the human ears ($20 - 20\,000$ Hz). Sound outside of this spectra, such as infrasound (< 20 Hz) and ultrasound ($> 20\,000$ Hz), have the same physical properties but cannot be heard by humans [10]. When sound interacts with light, the light may scatter and shift in frequency because of the acousto-optic effect [11]. Below is a simplified description of it. When the mechanical sound wave propagates through a medium, it induces an alternating pressure. An increased pressure increases the refractive index of the medium resulting in a, momentarily, lower

phase velocity for light passing through it. This will lead to a phase shift for the light. Since the sound will induce an oscillation between high and low pressure, so will the refracting index and further the phase shift. The phase shift oscillates by the same frequency as the sound and ads (or subtracts) this frequency shift to (from) the transmitted light.

2.3 Ultrasound optical tomography

The idea of using ultrasound to improve optical imaging methods was first presented in 1993 by Marks et al. [12]. The objective behind it was that tumor tissue and dense breast tissue have similar radiodensities, making small tumors hard to identify in ordinary X-ray mammography. With light, one was hoping to achieve enough contrast to be able to characterize the different tissue types. The limiting factors of using light as an imaging tool is the large absorption and scattering in human tissue. The effect of absorption can be minimized by using wavelengths in the optical tissue window but the scattering aggravates the backtracking of photons. This results in it being hard to identify the route of the light and the absorption along its path to the detector. UOT uses a pulsed ultrasound wave to "tag" photons in a specific area to overcome this problem. Since ultrasound has much lower scattering, it is possible to limit the size and position of the tagging area. By only collecting tagged photons and measuring their intensity, one can get a measurement of the absorption in the area. By moving this area, it is possible to construct an image of the absorption in the medium. An overview of the UOT-principle and light tagging can be seen in Figure 2.2.

2.3.1 Light-tagging

Light and ultrasound of frequency f_{L} and f_{US} respectively, is applied to the tissue. The ultrasound pulse changes the refractive index at its position making the light propagating through the volume occupied by the pulse shift in frequency, via the acousto-optical effect. This shift creates sidebands, of frequency f_{sideband}, to the carrier wave in the light signal. The light in the sideband is what is referred to as "tagged" light and has the frequency $f_{\mathrm{sideband}} = f_{\mathrm{L}} + nf_{\mathrm{US}}$, where n is a non-zero integer.

2.3.2 Rear-earth-ion-doped filters

One challenge in UOT is separating tagged photons from the untagged. The tagged photons constitute only a small fraction of all photons and the carrier and the tagged light signals are close in frequency making them harder to separate. The f_{L} is within the optical tissue window leading to a frequency of $\sim$400 THz and the f_{US} has the frequency of medical ultrasounds which is close to $\sim$3 MHz.

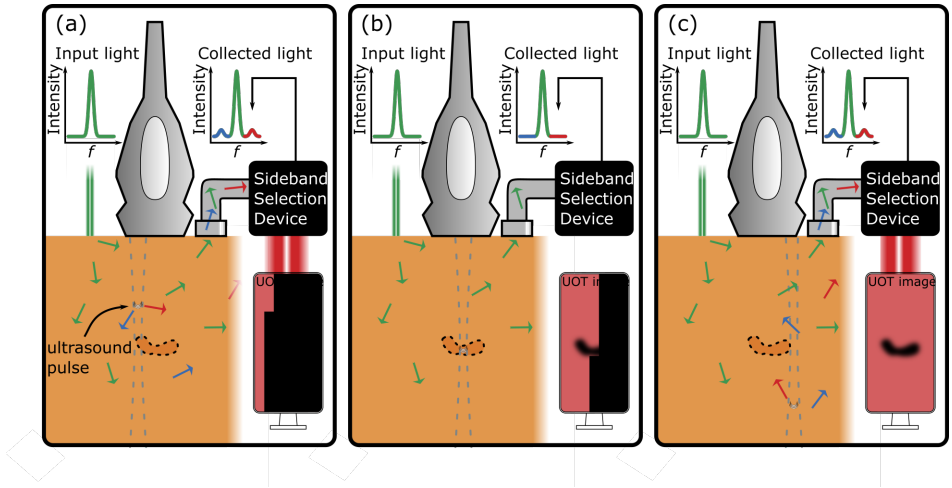

Figure 2.2: Overview of the UOT-principle from Hill [3]. (a) A tissue sample is illuminated with light of frequency f_{L}, presented as green arrows in the tissue. Some of the light interacts with the US-pulse, which tags it, and creates sidebands. The frequency of this light, f_{sideband}, presented as blue and red arrows, is collected together with the carrier wave. Only selecting one of the sidebands for imaging shows a constant absorption at this point in the scanning. (b) The US-pulse has reached a tumor, with higher absorption, resulting in the amount tagged light being reduced due to it being absorbed. This results in a shadow in the image. (c) Scanning through all positions creates an image of the varying optical absorption in the tissue.

The challenge is to separate the sideband frequency $f_{\mathrm{L}} \pm f_{\mathrm{US}}$ from the carrier frequency of f_{L}, or in numbers, separate the 400 000 000 $\pm$ 3 MHz signal from the 400 000 000 MHz signal. The research group at the Division of Atomic Physics at Lund University is using crystals doped with rear-earth-ions to produce long lived and sharp filters (<1 MHz wide). More on rare-earth crystals and their applications can be read in Bengtsson [13] and Sun [14].

Signal-to-Noise Ratio

To assure imaging of satisfying quality, the signal strength needs to be significantly high or, more specifically, the signal-to-noise ratio (SNR). Light detectors typically experience three different kinds of noise: shot-noise, readout noise and dark noise [15]. The detectors used at the Division today are single photon detectors which minimizes the readout noise and dark noise making the shot-noise the dominant contributor. Shot-noise is the fundamental noise of all light-sources and has a Poisson distributed shape. Increasing the signal will increase the noise proportionally to the square root of the number of photons in the signal. This reduces the SNR of a shot-noise limited detector to

$$\text{SNR} = \frac{\text{Signal}}{\text{Noise}} = \frac{N}{\sqrt{N}} = \sqrt{N} \tag{2.5}$$

where N is the number of photons in the signal.

Contrast-to-Noise Ratio in the shot-noise regime

A more demanding issue in UOT, and many other medical imaging methods, is to obtain sufficient contrast to be able to distinguish different tissue types. The different absorptions must lead to a large enough difference in signal and the variation in signal from within one tissue type should not be large enough to interfere with the imaging. We therefore define the contrast-to-noise ratio (CNR) as

$$\text{CNR} = \frac{\text{Contrast}}{\text{Noise}} = \frac{|S_A - S_B|}{\sqrt{\sigma_A^2 + \sigma_B^2}} \tag{2.6}$$

where S_A and S_B are the signals from two tissue regions called A and B. The standard deviation in signals for the regions are σ_A and σ_B. Rare-earth crystals has been shown to give promising results in theory [16] and by using this filtering method, the CNR can been described with the following equation

$$\text{CNR} = \sqrt{2S\eta}\frac{|N_A - N_B|}{\sqrt{N_A + N_B + T_U N_U}}. \tag{2.7}$$

In Equation 2.7, N_A and N_B refers to the number of tagged photons in the first sideband emitted from the tissue per unit area. The variable S is the size of the detector area and η is the detection efficiency (including losses from tissue to detected and quantum efficiency of the detector). T_U describes the filtering efficiency and is the fraction of untagged photons reaching the detector, and N_U is the number of emitted untagged photons from an area, i.e. the photons in the carrier wave that depends on how many have interacted with the ultrasound.

2.3.3 Medical safety limits

Even though UOT does not use any ionizing radiation there are still boundaries regarding medical safety that need to be taken into consideration when designing a UOT-system. An increased light exposure will increase the signal and improve SNR but might harm the tissue. The maximum permissible exposure (MPE) sets the limits for how much light the tissue can be exposed to and is divided into two thresholds. The first limits the safe maximum intensity of a pulse to 30 mJ/cm^2 [17]. If this exposure limit is exceeded, the tissue might take thermal

damage, causing necrosis. The second limits how high average power can be tolerated over time, which depends on the transportation capacity of heat in the tissue. The maximum tolerated MPE over time is 300 mW/cm^2 and, if exceeded photochemical and thermal injuries might be induced. A UOT-system uses laser pulses and must therefore take both restrictions into consideration. These presented MPE thresholds are for skin tissue. Different limits are applied to other tissue types with eyes being the most sensitive.

2.4 Simulation tool

A simulation code, *tagged-light-simulator*, written by Hill [18] and available for open source usage was used for the photon path modelling and light-sound interaction. The model simulates the acoustical and optical propagation and interaction in a medium using the Monte Carlo method.

2.4.1 Monte Carlo Simulation

To be able to model the propagation of light in tissue, the Monte Carlo (MC) model has been demonstrated to accomplish satisfying results [8]. The Monte Carlo method was implemented to simulate stochastic processes in large numbers, and has found several applications within statistics, mathematics and engineering [19]. The propagation of one single photon is well described and can easily be simulated [4, 8]. However, to simulate enough photons to be able to model light propagation sets high demands on computational power. Wang et al. [20] were the first to introduce a Monte Carlo model in multi-layered tissues (MCML) in standard C programming language, thus making the method widely available. It also sets the foundation for the algorithm used in this thesis.

2.4.2 UOT-simulation

The simulation tool synthesizes a tissue sample with optical parameters and a defined light-source and detector. The medium is divided into a number of three-dimensional pixels, or voxels, each with required optical parameter values for μ_a, μ_s and g. A light source from where the photons enter the medium is defined as either a point-source or a 'tophat'-distribution with a specified radius. The position and direction of the source and incoming photons are also decided. Further, the method for detection of photons can be defined as a circular detector with specified radius. From hereon the photon paths from light-source to detector can be simulated. Z number of photons are initialized somewhere in the light-source area and then propagate in the medium according to the rules described in Wang and Wu [4] until they hit the detector or leave the medium. Note that the simulation does not take the absorption, μ_a, into account at this point. The

paths of the photons that reach the detector, numbered M, are saved for further processing making the fraction of photons hitting the detector M/Z. From each completed path m, the model calculates the distance $d_{m,n}$, propagated in voxel n. N is the total number of voxels. All d values are stored in a matrix $\mathbf{D}$:

$$\mathbf{D} = \begin{pmatrix} d_{1,1} & \cdots & d_{1,n} & \cdots & d_{1,N} \\ \vdots & \ddots & & & \\ d_{m,1} & & d_{m,n} & & \vdots \\ \vdots & & & \ddots & \\ d_{M,1} & & \cdots & & d_{M,N} \end{pmatrix} \tag{2.8}$$

where each row refers to a completed photon path and each column to a voxel in the medium. Each path also defines an interaction spectra. From each spectra, the energy in the first sideband can be extracted as $a_{n',m}$ for each ultrasound position n'. Using this energy, a matrix containing the energy of each path and each ultrasound position is constructed. This matrix, $\mathbf{A}$ can be seen bellow:

$$\mathbf{A} = \begin{pmatrix} a_{1,1} & \cdots & a_{1,m} & \cdots & a_{1,M} \\ \vdots & \ddots & & & \\ a_{n',1} & & a_{n',m} & & \vdots \\ \vdots & & & \ddots & \\ a_{N',1} & & \cdots & & a_{N',M} \end{pmatrix}. \tag{2.9}$$

$\mathbf{D}$ and $\mathbf{A}$ together yield the UOT-image as

$$\mathbf{F} = \mathbf{A} \exp(-\mathbf{D}\boldsymbol{\mu}_a) \tag{2.10}$$

where $\boldsymbol{\mu}_a$ is the vector of absorption coefficients for each voxel in the medium and exp denotes the elemental-wise application of the exponential function. $\mathbf{D}$ is of size $(M \times N)$ and $\boldsymbol{\mu}_a$ of size $(N \times 1)$ and together they represent the absorption of each photon path. Together with $\mathbf{A}$, of size $(N' \times M)$, the UOT-image $\mathbf{F}$, of size $(N' \times 1)$ can be calculated.

2.4.3 Absorption reconstruction

Calculating $\mathbf{A}$ and $\mathbf{D}$ is comprehensive since hundreds of millions of photons need to be simulated, and altering $\boldsymbol{\mu}_s$ or $\mathbf{g}$ would require a new simulation. However, if $\mathbf{A}$ and $\mathbf{D}$ are determined and $\boldsymbol{\mu}_a$ is altered a new $\mathbf{F}$ can be quickly calculated since it only requires two matrix multiplications. This opens up for reconstruction tools [21]. Assuming a homogeneous, or static, scattering and

anisotropy, several $\boldsymbol{\mu}_a$ can be tested for a fix $\mathbf{A}$ and $\mathbf{D}$ to fit a measured image. This can be described by minimizing the objective function

$$\Omega(\mu_a) = ||\eta \mathbf{F}(\boldsymbol{\mu}_a) - \mathbf{b}||^2 \tag{2.11}$$

where $\mathbf{b}$ is the experimental image that $\mathbf{F}$ should be matched to and η is the experimental losses from detection the area at the tissue to the detector. In this way, a simplified reconstruction of the tissue absorption can be calculated.

3 Methods

The section aims to describe how the data and system were prepared and what simulations that were carried through.

3.1 Breast tissue phantoms

One of the goals of this thesis was to test the UOT concept for breast tissue models. Predrag Bakic, from the Department of Translational Medicine, Lund University and Skåne University Hospital, provided the project with *in silico* models of breast tissue mainly used for mammography analysis. These models were turned into optical models by giving each voxel optical parameters and then preprocessed before being used in the UOT-system.

3.1.1 Optical parameters

Optical parameter values from experiments on female breasts were used for the simulation to mimic human tissue. More specifically, values for μ_a, μ_s and g for the different tissue types in the breast.

The breast models provided by the Department of Radiology Translational Medicine, Skåne University Hospital, were three-dimensional models of breasts in the compressed position during mammography. The models were made of voxels, each classified as a tissue type. The tissue types in the models were: skin, adipose (fat), glandular, fibrous and tumor tissue. Since the breast is not block shaped, some voxels where also labeled as air. In an ideal case, optical parameters for each of the tissue types for the same wavelength in the optical tissue window should be used. Measuring optical parameters for specific *in vivo* (living) tissues is however a challenging task and, as such, few experimental demonstrations of this exist [22, 23]. Previous experiments have established that *ex vivo* results can differ a factor $\sim$10 from *in vivo* measurements, reducing the reliability of *ex vivo* measurements [24]. *In vivo* measurements does however exist on a bulk tissue level for the entire breast [22, 23]. To make use of our detailed breast models, some *ex vivo* results were used to establish the relation between the parameters of different tissue types [25].

The scattering coefficient, μ_s, and scattering direction distribution, g, are hard to measure experimentally leading to most scientific articles only presenting the reduced scattering parameter, μ_s' [9]. The simulation tool used in these simulations requires μ_s and g as separate factors. Previous experiments indicate that

g is ∼0.9 for most biological tissues and by using this value for our simulations, μ_s should be 10 times larger than μ_s' according to Equation 2.4 [4].

When optical properties are examined it is often for a certain wavelength. In this study, optical properties from several articles had to be used resulting in a wavelength mismatch. In this case, the optical parameters were linearly interpolated between the two closest wavelengths to match the decided wavelength.

The wavelength decided upon was 800 nm since it is in the optical tissue window and in the middle of the tested wavelengths in the articles. The main *in vivo* optical properties for bulk breast tissue were obtained from Durduran et al. [22]. To get a more detailed model, *ex vivo* data on the optical properties for adipose and glandular tissue from an article by Peters et al. [25] was used. The data showed that the absorption of glandular was 67 % compared to the absorption of adipose and the scattering of glandular was 165 % of the scattering of adipose. This data, however, did not present optical properties for fibrous tissue, and here it is therefore for simplicity assumed to have the same optical properties as glandular tissue. Adipose and glandular/fibrous tissue form the majority of the tissue (∼95 % in our model) in the breast. The contribution of each of the two for the bulk tissue was assumed to be linear meaning that the average of the two should, with taking concentration into account, become the bulk tissue values. Finally, the *in vivo* optical properties for skin and tumor tissues were obtained from Sandell and Zhu [23].

From the information earlier, the optical parameters used in the simulation is presented in Table 3.1. The data displays that the absorption and scattering for tumor tissue is ∼2 times larger than the bulk tissue.

Table 3.1: Optical properties for the tissue types in breast tissue for 800 nm used in the simulations [22, 23, 25].

Tissue type	μ_a [cm^{-1}]	μ_s [cm^{-1}]	μ_s' [cm^{-1}]	g [unitless]
Skin [23]	0.19	73	7.3	0.9
Adipose [22, 25]	0.047	72	7.2	0.9
Glandular & fibrous [22, 25]	0.031	120	12	0.9
Tumor [23]	0.085	140	14	0.9
Bulk tissue [22]	0.043	84	8.4	0.9

3.1.2 Pre-processing

Producing light paths using the MC-method and simulating light-sound interaction is computational heavy making pre-processing and optimization important. In order to reduce calculation time for the simulation, the optical models were pre-processed and down sampled. The experiments performed at the Department of Atomic Physics today uses a 4 cm wide linear US-transducer, and to

match any potential experiments, the imaging was limited to the same width. A sample with a dimension of $5 \times 5 \times 5$ cm was cut out of the original tissue model for the light modelling to have room for photons diffusing beyond the imaging field. This can be seen in Figure 3.1.

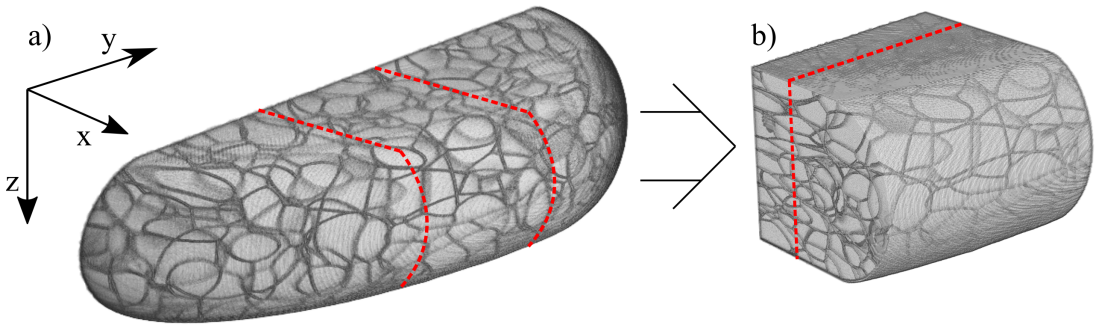

Figure 3.1: Image of the initial pre-processing of the breast tissue phantom. a) The figure shows the original simulated tissue sample with the $5 \times 5 \times 5$ cm cutout marked in red. b) The figure shows the $5 \times 5 \times 5$ cm cutout from a) with the plane to be imaged marked.

UOT is advantageous in deep tissue imaging compared to other optical imaging methods such as photo-acoustic tomography (PAT) [26]. The photon path simulation was performed on the $5 \times 5 \times 5$ cm medium but to reduce calculation time for the light-sound interaction, the most superficial 0.5 cm on the top and bottom side were cut out of the UOT-simulation making the final image 4×4 cm. The physiological models had a resolution and voxel size of 0.2 mm whereas the US, which limits the resolution of UOT, has a resolution closer to $\sim$1 mm. All parameters in the optical models were therefore linearly down sampled to a voxel size of $\sim$1.3 mm. This balances the resolution with simulation time. The process can be seen in Figure 3.2.

3.2 Simulation set-up

UOT can be done in two generalized geometries, reflection and transmission mode. In reflection mode, the light-source and detector are on the same side of the medium and in transmission mode, they are on opposite sides.

3.2.1 Transmission geometry

For reflection mode, the signal is strong in low penetration depths and weak in deep, since the light needs to propagate from the source to the tagging area and then back again to the detector. With transmission geometry, the signal is much more even since all photons must propagate through the tissue to reach the detector, independent of where the tagging occurs. Even if reflection mode has

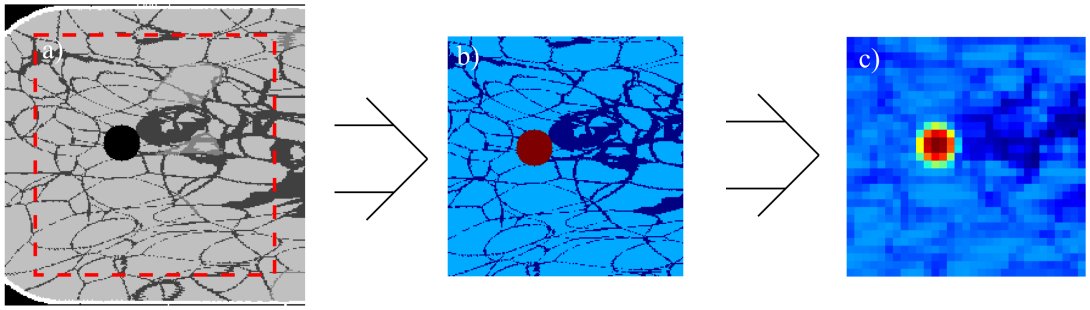

Figure 3.2: Image of down sampling of a breast tissue phantom with a tumor. a) The figure shows the original image cutout that was marked in Figure 3.1b. Each color refers to a tissue type: skin (white), adipose (light gray), glandular/fibrous (shades of gray) and tumor/air (black). The 4×4 cm area to be imaged in the UOT-simulation is high-lighted. b) The 4×4 cm slice with each tissue type assigned the absorption coefficient from Table 3.1. c) The absorption image down scaled to a pixel size of 1.3×1.3 mm. Note that the same pre-processing is done for the scattering.

the fewer utilization restrictions, since all sensors can be equipped in the same probe and only one free surface is needed for imaging, a transmission geometry could be preferable for specific applications. One such case is mammography, were the breast is compressed between two plates that could include a light-source on one side and detector on the other. Imaging breast tissue with UOT is also suitable as high absorbing tumors would give high contrast to the low absorbing breast tissue. The distance from light-source to detector would be $\sim$5 cm which is within the imaging depth of UOT.

3.2.2 Light configuration

In order to improve the image taking conditions for larger two-dimensional images, new light configurations were tested. UOT images different intensities in light, due to varying absorption. Therefore, an even light distribution in the imaging window could even out the noise map from different parts in the image and improve CNR. This can be conducted in two ways, first: by injecting the light onto a larger tissue area. Second: by increasing the uptake of light. These improvements can be done by adding light sources and detectors, or by increasing their area. Since the threshold for MPE is in $\mathrm{mW/cm^2}$, an increased input area can also increase the total power without risking to harm the patient.

A downside of increasing the input and output area is an increment in untagged light. When the concentration of tagged light falls, as the light comes from a wider region of tissue, the CNR decreases.

3.2.3 Light intensity

Since the images show the intensity of tagged outgoing light, knowledge of the incoming light is of importance. The final image was a 4×4 cm image with a resolution of 1.3 mm, which means that the size of the model is 31×31 pixels, or 961 in total. In this simulation we used a continuous wave ultrasound and laser where the ultrasound sent one pulse at a time for each of the column of pixels or "lines". The laser was turned on when the US-pulse reached the first pixel, at depth 5 mm, and stayed on as the pulse propagated through the tissue. When it reached the end of the imaged area, at depth 45 mm, the laser was turned off. The US-pulse continued, reached the end of the tissue sample, reflected at the edge and faded off in the tissue before the next pulse was sent in for the second line. This continued for each of the 31 US-pulse paths, or lines. The confinement of tagged photons to a certain depth in the tissue was done by knowing the position of the ultrasound through the propagation speed. Ultrasound has a propagation speed of 1.48 mm/µs in breast tissue making the travelling distance of 40 mm in the image take 27 µs [27]. The cooldown between pulses was set to 80 µs in order to let the US-wave fade off and prevent overheating of the US-transducer. This led to the fraction of time with the laser active $\frac{27}{80} = 0.3375$. To reach a high SNR, the light power should be as large as possible. Since the MPE over time is 300 mW/cm^2 and the laser was active for 33.75% of the time, the light could be injected with a power $P_0 = \frac{300}{0.3375} \approx 890$ mW/cm^2 and stay within the safety limits. This remains well within the maximum intensity of a pulse since the max power is 890 mW/cm^2 and during one line of illumination the energy reaches $890\,\text{mW/cm}^2 \times 27$ µs $= 24.0$ µJ/cm^2 which is significantly lower than the limit of 30 mJ/cm^2.

The number of photons emitted is also relevant when calculating SNR and CNR. The energy of a photon depends on the wavelength of the light and can be calculated with

$$E_{\text{photon}} = \frac{h \times c_\circ}{\lambda} \tag{3.1}$$

where h is Planck's constant, $c_\circ$ is the speed of light in vacuum and λ the wavelength of the light. During 1 s of continuous image taking with described set-up with maximum power and wavelength 800 nm, the number of emitted photons for a 1 cm^2 light-source equals $\sim 10^{18}$ photons per image or 10^{15} photons for each pixel in the image.

3.2.4 Used parameters

The simulations were done with different light configurations but the simulations parameters remained the same during all simulations. This included how many photons to be simulated, the wavelength and the shape of the ultrasound pulse. The number of photon paths M was set to 100 000, the light wavelength to 800 nm and the US-frequency f_{US} to 3 MHz. To characterize the ultrasound pulse the full width half max was set to 3 mm and the peak pressure to 1 MPa.

Optimize runtime

The calculation of UOT-images is computationally heavy and optimizations are made where possible. The system uses a fast Fourier transform (FFT) to calculate the frequency spectrum of the signal and separate the tagged signal. To make the FFT more efficient, three parameters were taken into consideration. The first parameter is the number of points S the time should be divided into. For the computation to be efficient, S should be a power of 2. The second parameter Q is the number of segments each free path length is divided into. The third parameter, the sampling frequency, f_{s}, should be at least 2 times larger than the frequency it is detecting, f_{US}, to avoid aliasing according to the Nyquist theorem. To identify the optimal parameter values, large values were initially tested for a few tagged photon paths and gradually decreased until the pulse shape at the frequency spectra changed dramatically. This reduced the resolution to the minimum while the crucial characteristics were still preserved. The parameters were set to $S = 2^7$, $Q = 3$ and f_{s} to $6f_{\mathrm{US}}$.

3.3 Light distribution analysis

Simulations with three different optical set-ups were performed to evaluate the effect on the resulting image and can be seen in Table 3.2 and in Figure 3.3. The light-source was placed on top of the tissue and the detector directly under it, 5 cm apart. The ultrasound transducer was also centered at the top and was therefore overlapping the light-source. Such a construction will be difficult to accomplish in reality but this gives optimal circumstances for the system to produce reliable results. This facilitates the comparison of the cases which is the focus of this thesis.

Case 1 simulated a circular light-source and detector with maximized power allowed by MPE. Case 2 simulated a rectangular 4×1 cm light-source and a detector divided into two smaller detectors separated by 2 cm. The total light power was the same as for Case 1. This led to the light distribution being more even and can increase the image quality, independent from the advantage of increased signal when a larger input is used. The simulation in Case 3 was identical to Case 2 apart from a four times higher light power. This was performed to evaluate the full effect of changing the configuration. The phantom used in all simulations was a breast tissue sample with a tumor and the simulations were compared regarding SNR and CNR. The required parameters for CNR-calculations that could not be defined from our simulations were obtained from previous studies by Bengtsson et al. [16]. This included the parameter values $\eta = 0.075$ and $T_U = -30$ dB. In all three cases, the detector area was $S = 1$ cm^2. No clear separation of the tissue types A and B could be defined since a voxel may contain parts of both tissue types due to the down sampling. Therefore, the signal from region A was decided to be the UOT-signal from the

breast tissue. The signal from region B, was obtained from a UOT-simulation of a "blank" tissue sample, with the homogeneous absorption and scattering of bulk breast tissue.

Table 3.2: Tested cases in the light distribution analysis.

	Case 1	Case 2	Case 3
Light-source	Circle, 1 cm^2	Rectangle, 4 cm^2	Rectangle, 4 cm^2
Detector	Circle, 1 cm^2	2 circles, 0.5 cm^2 each	2 circles, 0.5 cm^2 each
Power	890 mW	890 mW	3560 mW

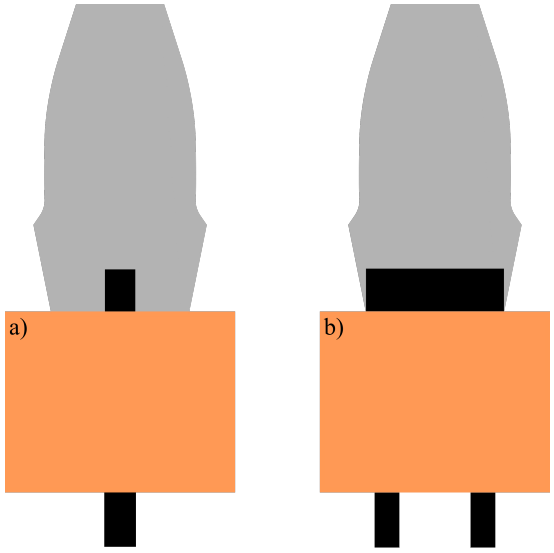

Figure 3.3: Image of the set-up for a) Case 1 and b) Case 2 described in Table 3.2. The gray ultrasound transducer and black light-source are placed on top of the tissue and the black detectors are placed under it. Note that the set-up for Case 3 is the same as for Case 2 but with a higher power.

Simulation tool modifications

In order to simulate with the set-up explained, some changes had to be done to the simulation tool. A new light-source was implemented to get a rectangle shape input with homogeneous light distribution. The divided detector was also implemented to be able to have two detection areas.

3.4 Image reconstruction analysis

The purpose of UOT is to find and identify changes in absorption, but as the light distribution and raw signal is highly affected by the configuration of input

and output, tools were developed in order to help the evaluation of image content. The simulation only simulated shot-noise and no other variations in the signal resulting in Case 3 only being a scaling of Case 2. This still affect the theoretical SNR and CNR for the cases but will not differentiate the reconstructions. Therefore, only Case 1 and Case 2 will be presented in the reconstruction analyses.

3.4.1 Ratio reconstruction

One method to reconstruct the absorption in the tissue and to identify abnormalities in the signal is to compare the results with the signal from a blank tissue. To do this, a UOT-simulation was performed on a breast tissue sample with the optical set-up for Case 1 and 2 in Table 3.2. Thereafter a similar simulation was performed with the same set-up on a blank tissue sample, with the homogeneous optical parameters from bulk breast tissue. The two resulting UOT-signals, $\mathbf{F}_{\text{breast}}$ and $\mathbf{F}_{\text{blank}}$, were divided by each other to get the ratio $\frac{\mathbf{F}_{\text{blank}}}{\mathbf{F}_{\text{breast}}}$. In this way, deviations in the breast tissue sample was enhanced in the resulting image.

3.4.2 Absorption reconstruction

Another method to evaluate the signal content is to use the advantage of computationally cheap absorption altering described in Section 2.4.3. The tool uses the same signals as in the ratio reconstruction, $\mathbf{F}_{\text{breast}}$ and $\mathbf{F}_{\text{blank}}$, but instead tries to match the absorption in the blank tissue sample to alter $\mathbf{F}_{\text{blank}}$ to match $\mathbf{F}_{\text{breast}}$. The scattering remained static. $\mathbf{F}_{\text{breast}}$ was used as the experimental variable $\mathbf{b}$ in Equation 2.11. The blank signal needed further pre-processing since $\mathbf{b}$ only images the central 4×4 cm, and these voxels should be the one to affect the reconstructed signal. Voxels outside of this window does however affect the photon paths and for the reconstruction to focus on reconstructing the voxels in the central image, all other voxels in the $5 \times 5 \times 5$ cm tissue sample were simplified to have the same absorption. This limited detailed variations to the imaged signal. In practice, this is done by summation of the columns in $\mathbf{D}$ that do not refer to one of the voxels in image $\mathbf{b}$. The $\mathbf{A}$ and new $\mathbf{D}$ were used with different absorptions to minimize $\Omega(\boldsymbol{\mu}_a)$ in Equation 2.11 using the Levenberg-Marquardt algorithm for 30 iterations [28, 29]. Since both images are synthesized with the same simulation tool, the losses from tissue to detector was the same and η was therefore set to 1. To only get realistic absorption parameters, the reconstruction was limited to only use values between 0.01 cm^{-1} and 0.5 cm^{-1}.

4 Results

4.1 Tissue images

Various techniques were tested to see how tissue can be imaged with UOT-methodology. The absorption and scattering in the breast tissue sample is presented in Figure 4.1 and can be used as reference when analyzing the different techniques. The figure images a tumor with large absorption and scattering. A larger concentration of fibrous/dense tissue to the right of the tumor has resulted in higher scattering even-though the absorption is relatively even. Note that the following images originates from these "ground truth" values and this is what a reconstruction would look like in an optimal case.

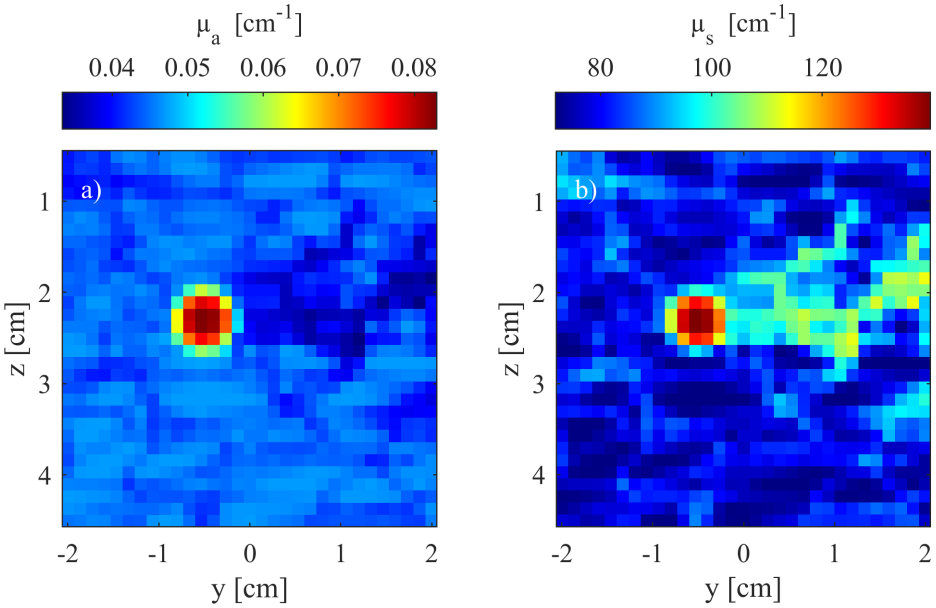

Figure 4.1: Image of the absorption and scattering coefficients for the breast tissue sample. a) Shows the absorption coefficients. b) Shows the scattering coefficient.

4.2 Light distribution analysis

In order to compare how the different set-ups affect the light distribution in the tissue and further the UOT-images, the photon path distance in each voxel, or **D**, in the imaged 4×4 cm can be seen for Case 1 and Case 2 in Figure 4.2. In the images the light-source is centered at the top and detector at the bottom of and the slice is cut at $x = 0$. The first two images show the light distribution

of all photons entering and exiting the tissue and the second two only show the light distribution of the photons reaching the detector.

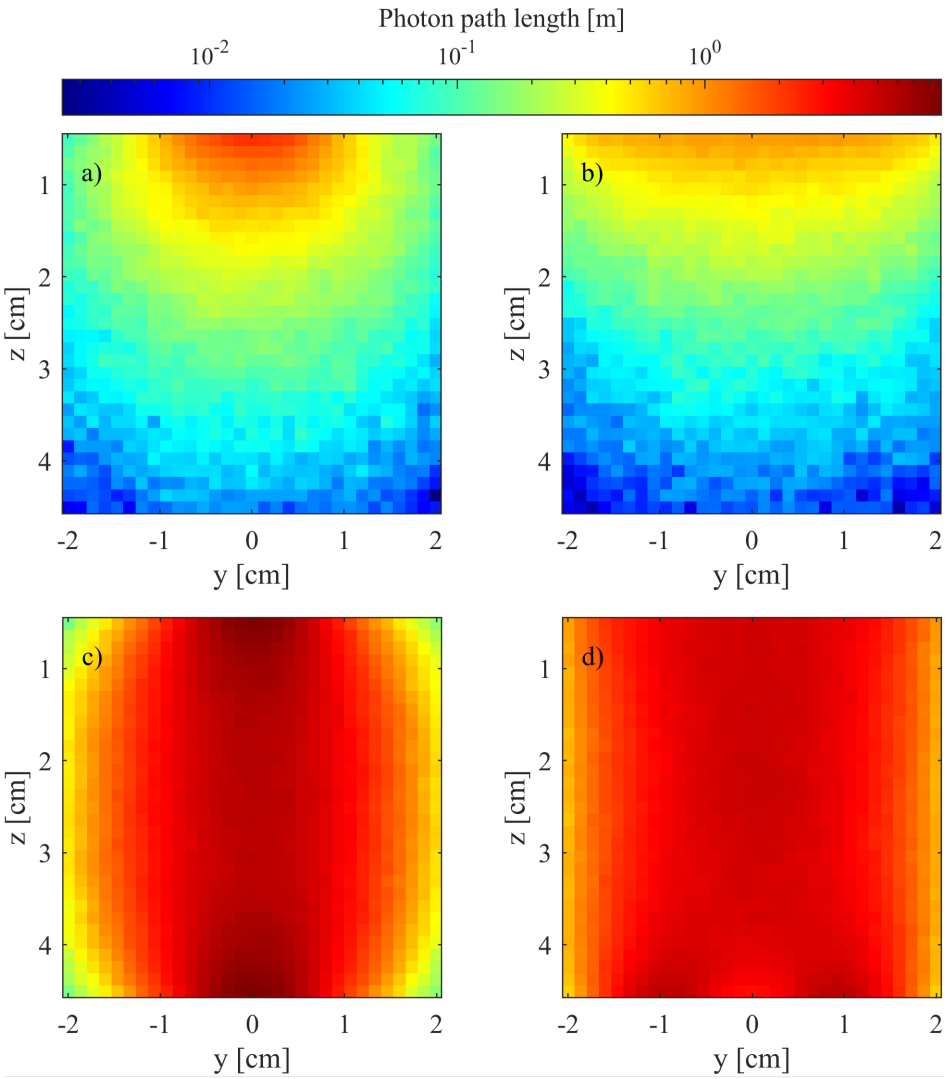

Figure 4.2: A visual representation of **D** that for a) and b) present the distribution of all photons entering and exiting the tissue, and for c) and d) only present the distribution of photons that reach the detector. a) and c) are simulated with Case 1 using a circular light-source and detector. b) and d) are simulated with Case 2 using a rectangular light-source and 2 smaller detectors. Note that the intensity scale is logarithmic

Figure 4.2c and d demonstrate that the intensity of light is largest close to the light-source, falls off deeper in the tissue and then intensifies again close to the detector. This is expected since the simulation images the photons reaching the detector and all photons are emitted from the light-source. With the wider source the light distribution is more even in the tissue. A more spread out light distribution, on the other hand, decreases the ratio of photons hitting the detector which can be seen in the number of emitted photons for the same number of detected photons in Table 4.1.

Table 4.1: Number of emitted photons in the UOT-simulation for the different set-ups. Note that M is constant at 100 000 for all cases.

	Case 1	Case 2 & 3
Z_{breast} (Nbr of photons)	194×10^6	302×10^6
Z_{blank} (Nbr of photons)	171×10^6	265×10^6

4.2.1 SNR and CNR

How the different cases affect the image in regards of SNR and CNR is presented in Figure 4.3 and 4.4. These images simulated 1 second of imaging on the breast tissue sample and the only noise included was the shot-noise. A CNR over 1 must be achieved in order to be able to detect contrast through the noise.

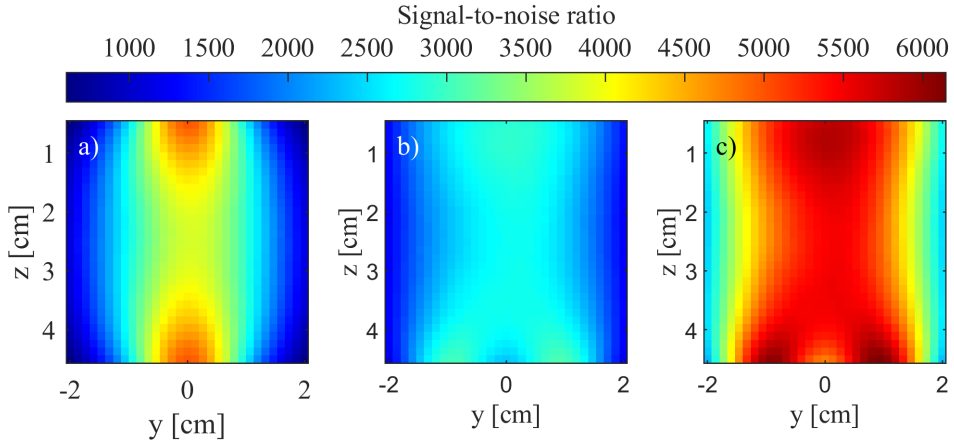

Figure 4.3: Image of the SNR in the first sideband for each pixel in the breast tissue. The figure presents the SNR for a) Case 1, b) Case 2 and c) Case 3.

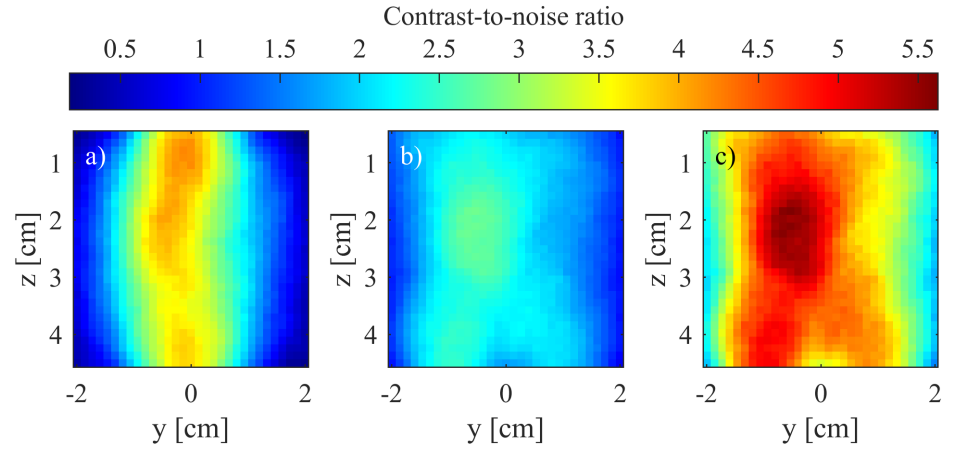

Figure 4.4: Image of the CNR in the first sideband for each pixel in the breast tissue. a) Case 1, mean: 2.2. b) Case 2, mean: 1.9. c) Case 3, mean: 3.8.

4.3 Image reconstruction analysis

From the light path simulation, the UOT-signal could be simulated. The signal in the first sideband from a UOT-simulation with the set-up from Case 1 and Case 2 and 1 second of imaging is presented for breast and blank tissue, with homogeneous absorption and scattering, in Figure 4.5. The breast image $\mathbf{F}_{\text{breast}}$ and blank image $\mathbf{F}_{\text{blank}}$ appear similar for each case and it is hard to observe any differences other than the slightly fewer photons in the breast tissue simulations. The signal is lower in Case 2 since Z was larger for this case resulting in a lower ratio of emitted photons reaching the detector. Case 1 does however show a lower signal for the most outer pixels on each side.

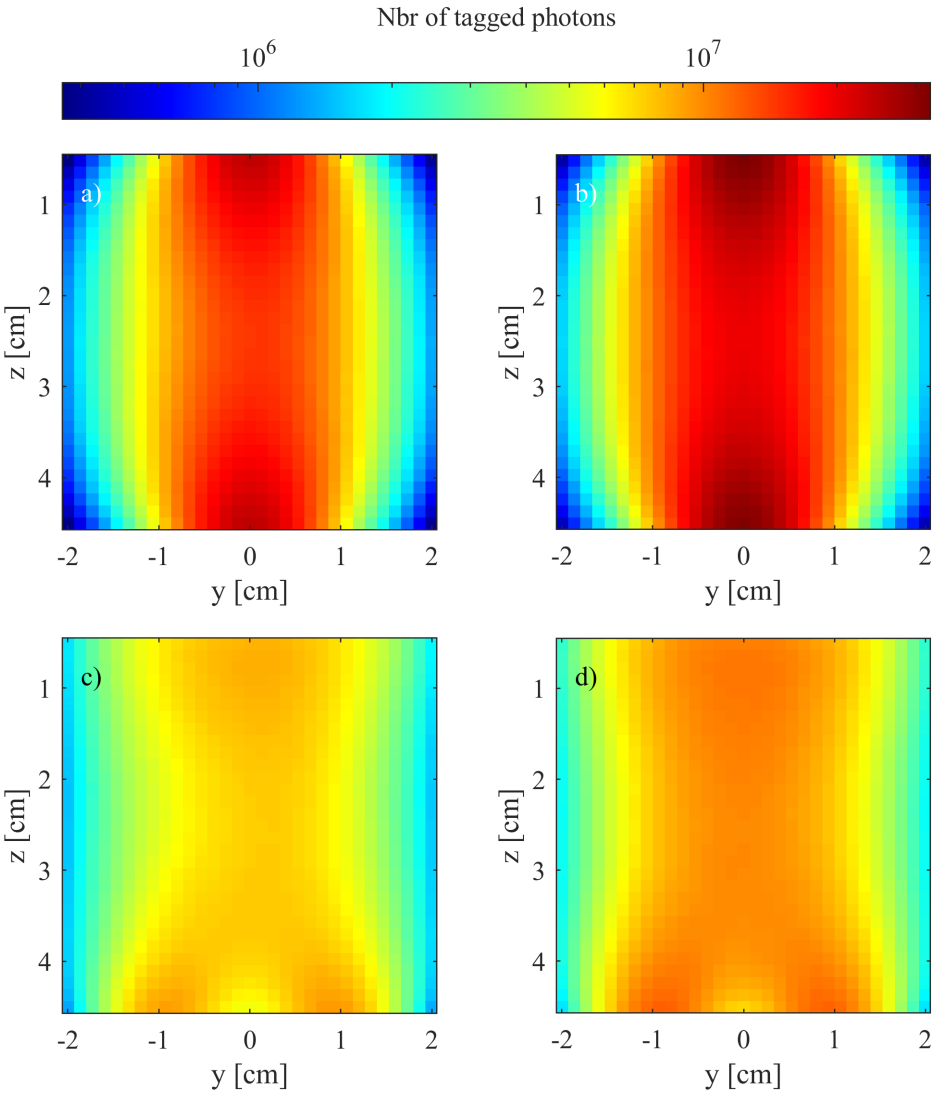

Figure 4.5: The signal $\mathbf{F}_{\text{sideband}}$ for Case 1 and Case 2 simulated on two tissue samples: one breast tissue sample and one "blank" tissue sample, with homogeneous abosrption and scattering. a) and b) show the signal from the breast tissue $\mathbf{F}_{\text{breast}}$ and blank tissue $\mathbf{F}_{\text{blank}}$ with Case 1 set-up. c) and d) show the signal from the breast tissue $\mathbf{F}_{\text{breast}}$ and blank tissue $\mathbf{F}_{\text{blank}}$ with Case 2 set-up.

4.3.1 Ratio reconstruction

To increase the visibility of abnormalities in the breast tissue image, Figure 4.6 presents the ratio $\frac{\mathbf{F}_{\text{blank}}}{\mathbf{F}_{\text{breast}}}$ for Case 1 and Case 2. The ratio is high at the position where the absorption is large in the breast image. Both cases indicate a large ratio at the area of the tumor and close to it.

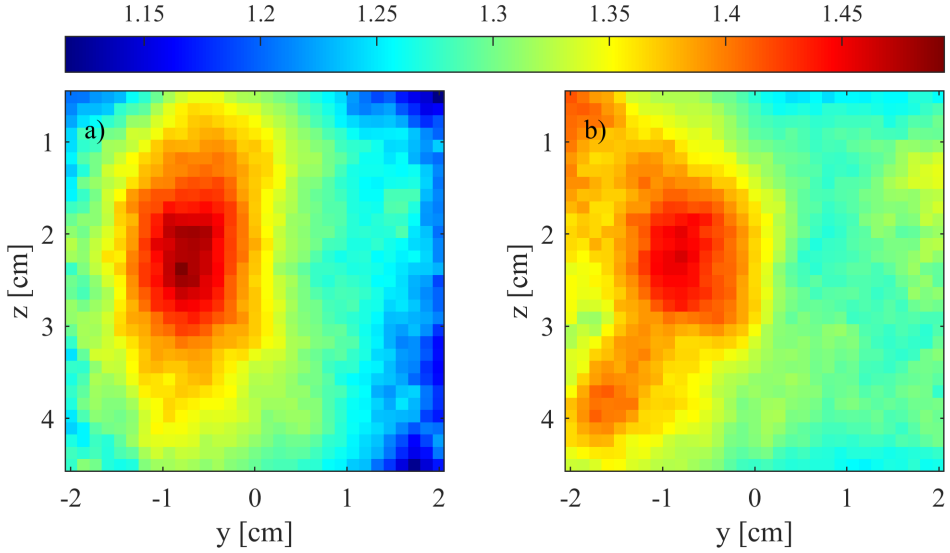

Figure 4.6: Image of the ratio $\frac{\mathbf{F}_{\text{blank}}}{\mathbf{F}_{\text{breast}}}$ from Figure 4.5. a) Presents the ratio using the configuration from Case 1. b) Presents the ratio using the configuration from Case 2.

4.3.2 Absorption reconstruction

The second reconstruction is made by altering the absorption in the blank tissue to get a signal that matches the one from the breast tissue sample as described is Section 2.4.3. The image in Figure 4.7 suggests the absorption $\boldsymbol{\mu}_a$ that best matches the signal for Case 1 and Case 2. The mean absorption $\langle \mu_a \rangle$ and error $\Omega(\boldsymbol{\mu}_a)$, from Equation 2.11, is also presented. Both cases identify the tumor but other areas of high absorption can also be seen for both cases.

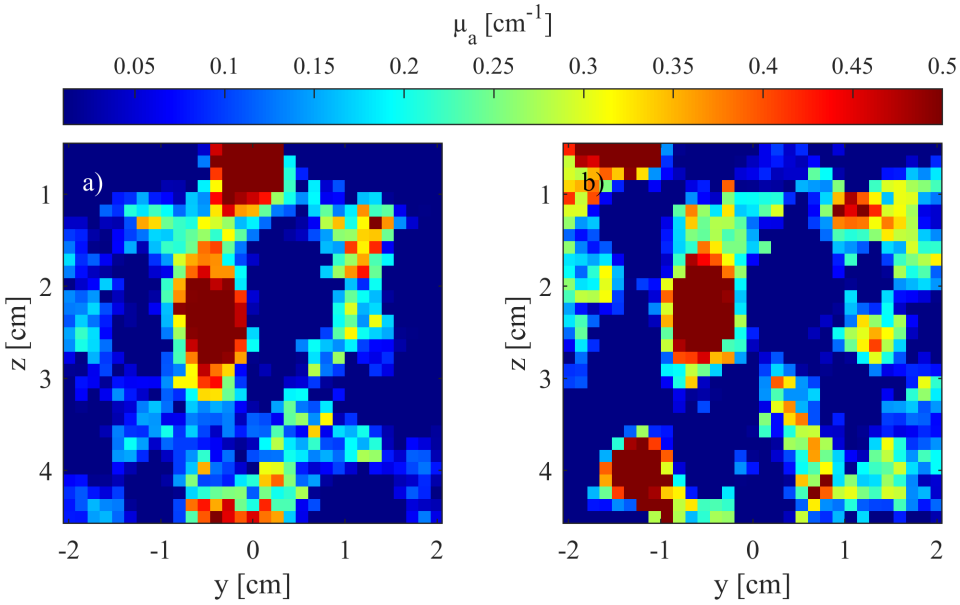

Figure 4.7: Image of the results using the absorption reconstruction method. a) Presents the reconstructed absorption for Case 1. $\langle \mu_a \rangle = 0.12$ cm^{-1}, $\Omega(\boldsymbol{\mu}_a) = 0.62$. b) Presents the reconstructed absorption for Case 2. $\langle \mu_a \rangle = 0.14$ cm^{-1}, $\Omega(\boldsymbol{\mu}_a) = 0.45$.

5 Discussion

5.1 Optical parameters

One remark that can be discussed is the selection of the optical parameters for the tissues. As mentioned in Section 3.1.1, some adjustments had to be made to complete a set of parameters for the analysis. There are several issues that can be discussed. Can the relationship between *ex vivo* parameters be used as guidance for *in vivo* parameters? Does using parameters from different sources increase the potential error? Can the parameters for a wavelength be simplified as the value in-between two nearby? These considerations are all relevant and affects the trustworthiness in regards of imitating the human tissue. More consideration could be taken when deciding upon the used parameters but the difficulties in obtaining accurate measurements for specific wavelengths remains a challenge and is the reason why it cannot be found in the literature. The different optical parameters for the tissue types incorporates irregularities which will cause variation in optical properties in the simulations. For humans, the shape and optical properties between individuals will vary which may result in absolute values being less important than relative values.

5.2 Optical set-ups

5.2.1 Compared set-ups

The decision to test different light configuration cases was made to compare how it may affect the resulting UOT-image. Case 1 was a simple case used as reference and the other cases to see if and by how much one could improve the images by changing the light configuration. To change the light-source and detector at the same time does however make it hard to see the contributing factor for each of them. In all simulated cases, the detector size remained the same. To change the size of the detector is an experimentally more demanding challenge than changing the size of the light-source. A larger photon collection area would increase the collected signal but would also require a larger rear-earth-ion-doped crystal and detector. The areas of the crystal and detector need to be at least as large as the light collection surfaces because diffused light cannot be focused without losing intensity. If the crystal and detector remain the same and the collection area is doubled, the intensity from each of the two collectors would be reduced to half when overlapped in the crystal. Despite these remarks, the light configuration is still of interest and future experiments could be done to see how this may affect

the imaging results.

5.2.2 Emitted photons

The number of emitted photons, Z, for the cases in Table 4.1 indicated that the ratio of light reaching the detector when altering the configuration from Case 1 to Case 2 and Case 3 was decreased by $\sim$35 %. This reduces the effectiveness of the set-up in Case 2 and Case 3 and requires the total power to be increased in order to be able to compete with Case 1. The results also suggested that it takes fewer photons to reach M paths for the blank tissue compared to the breast tissue in both cases. Since the absorption is added at a later stage, the scattering is the cause. Both tissue samples have the same average scattering but the imaged slice have more fibrous/glandular tissue with high scattering, as can be seen in Figure 4.1b. This result in photons being scattered away from the detectors and more emission needed to reach M paths.

5.2.3 SNR and CNR comparison

The largest values for SNR and CNR can be seen in Case 3 in Figure 4.3 and Figure 4.4. The SNR comparison showed, as expected, largest values for the highest input and lower values for a smaller and diffused input. However, the CNR results are not as clear. All cases presented a CNR over 1 at the tumor position and close to the light-source and detector. This indicates that all set-ups will be able to detect the tumor through noise but Case 3 seems to have the highest amplitude. For Case 2 and Case 3, the largest CNR in the image was found at the position of the tumor and close to it. This is expected since the largest difference in signal should be at the area of largest absorption, which is at the tumor position. Case 1 also have a large CNR close to the tumor but showed the highest values close to the light-source. This is probably due to the high concentration of light and the overall difference between the breast and the blank tissues. For a more concentrated light, as for Case 1, a mismatch in scattering will lead to a large difference since the light will diffuse more in one of the cases. For a diffused input, as in Case 2 and Case 3, the difference will be smaller since the light will be diffused for both tissues, regardless of any mismatch in scattering. A large CNR close to the light-source indicates a risk for artefacts in images generated with this set-up and set high demands on the blank tissue to match the measured breast tissue. Even though Case 1 has a larger mean CNR than Case 2, Case 1 presents, at the edges, the lowest CNR which might limit the focus to only detect tumors in the central region. A diffused input can result in a larger imaging field with satisfactory contrast with the traded-off of lower contrast in the center of the image.

5.3 Reconstructions

The reconstructions were only performed using Case 1 and Case 2. With the used simulation method, Case 3 would appear the same as Case 2 because it only adds a scaling factor to the breast and blank images that would be neglected in the reconstructions. A model that simulates noise, other than shot-noise, would increase the complexity and differentiate Case 3 from Case 2.

5.3.1 Ratio reconstruction

Analyzing the results from the ratio reconstruction in Figure 4.6 demonstrated that both cases detected the tumor even though Case 2 displayed artifacts reaching from the upper and lower left corners to the tumor. The ratio reconstruction presented a higher peak intensity for Case 1 at the tumor position than for Case 2. The position and contrast were, on the contrary, less defined and the tumor took up a larger space compared to Case 2. This is an effect of the light configuration of the respective set-ups. For Case 1, the light propagated in the vertical direction in an oval shape, as can be seen in Figure 4.5a and b. As a result, the probability of light passing through the tumor and also passing through the pixels above and beneath it increases. This will lead to a lower signal for these areas which will show in the ratio reconstruction. The pixel next to the tumor in the y-direction is, on the other hand, not as affected since the probability of light passing through them and also through the tumor is lower. This explains why the experienced smoothing of the tumor was larger in the z-direction than the y-direction.

For Case 2, the light propagated in an hourglass shaped path, according to Figure 4.5c and d. Because the tumor was located left of the centre, the probability of photons originating from the left side of the light-source and photons reaching the left detector have a high probability of also propagating through the tumor resulting in a lower signal for these areas. This explains why the smoothing is reaching from the tumor to the left side corners. It can, nevertheless, be demonstrated that division by a reference image can enhance the detection capability of a tumor, or area of larger absorption, with both set-ups even though the size of the tumor remains poorly defined.

5.3.2 Absorption reconstruction

The resulting absorptions from the absorption reconstruction differed between the two cases, which can be seen in Figure 4.7. For Case 1, the tumor was detected but artefacts close to the light-source and detector could also be seen. For Case 2, the tumor was detected but the image suggested more clumped up artifacts. Two of them were the same as in the ratio reconstruction but three artefacts with less absorption could be seen in the right part of the image.

The reconstruction only alters the absorption and not the scattering and high scattering can lead to a more absorbed light since the photons in the voxels will travel a longer path before they reach the detector and therefore have more time to be absorbed. This probably plays a role in the artifacts in the right side for both cases. The artifacts at the left side in Case 2 probably has the same origin as the ones in the ratio reconstruction, namely the probability of photon that have reach these areas also have a high probability of propagating through the tumor.

Many absorption values in both cases have reached the predefined boundaries, both upper or lower. The probable reason for this is that a perfect reconstruction cannot be made for a homogeneous scattering and requires altering of μ_s and g. Therefore, extreme values might give the best solution. Expanding the boundaries would lead to a lower error, Ω, but also allow the reconstruction to reach absorptions that cannot be found in human tissue. Even though the absorption is overall higher than in the tissue sample in Figure 4.1, the method still highlights interesting areas in the image.

To see how the scattering affects the absorption reconstruction, a reconstruction of the breast tissue using the scattering of $\mathbf{F}_{\text{breast}}$, instead of $\mathbf{F}_{\text{blank}}$, as $\mathbf{F}(\boldsymbol{\mu}_a)$ can be seen in Figure 5.1. One could imagine that using the correct scattering would result in an ideal reconstruction of the image, but since the paths in the voxels outside the imaged plane are added together, the two models are no longer perfectly matched. The result presents the tumor with less artifacts but the absorption is not matching the absorption in 4.1a. The difference at the top- and bottom-most pixels is probably due to a combination of the artifacts in Case 2 discussed earlier and compensation for the larger absorption in the skin that is neglected in the averaging of all voxels outside of the central voxels.

The question why this simulation illustrate a more accurate representation, although the circumstances are optimal due to the perfect match in scattering, and what can be done to improve the reconstruction with the blank is raised. The difference in Z results in a difference of tagged photons between the breast and blank simulations. This might be a contributing factor but the role of the scattering is probably the dominant factor. The demonstration in Figure 5.1 shows that much of the performance of this method depend on the properties of the blank image. Including a set of blanks with different scattering is a further step in developing this method. This should be executed before determining the performance of this method.

5.3.3 Future reconstruction improvements

Both reconstruction models use blank images as reference. The absorption and scattering in these were the same as for bulk tissue but this does not necessarily need to be the best option for reconstruction. A set of pre-simulated blank images, with varying scattering and absorption, to alter between could be used in

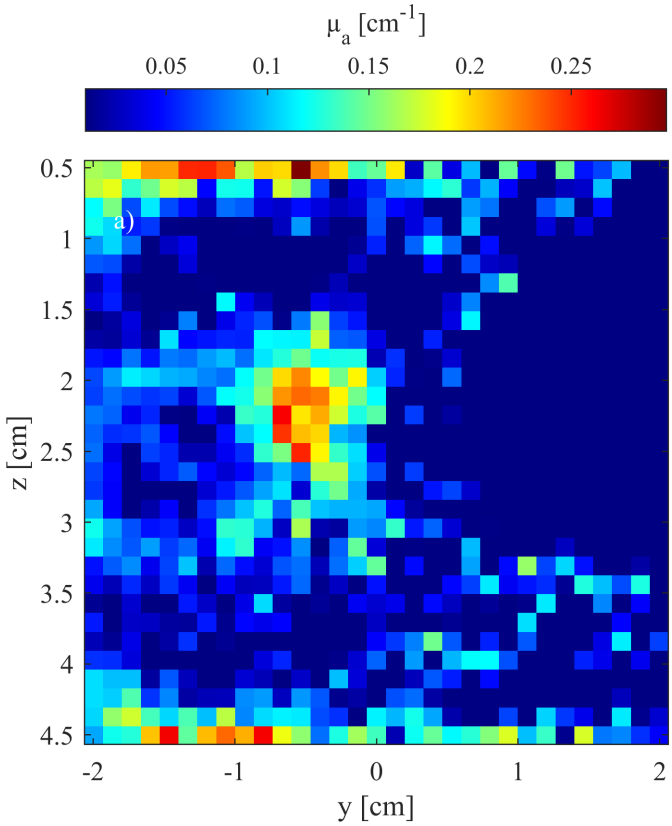

Figure 5.1: Image of the results from the absorption reconstruction of the breast tissue with a tumor when the same breast tissue with a tumor was used as reference. The reconstruction shows the result using Case 2 set-up. $\langle \mu_a \rangle = 0.05$ cm^{-1}, $\Omega = 0.036$.

the reconstructions to see which enhances the image the most. One must also be humble that selecting a blank image with high performance to estimate a correct representation of the tissue may not be as easy as in simulations. Difference in breast density and variation between patients will set high demands and require careful selection.

The two reconstruction methods presented different results but both detected the tumor. One way of improving the ratio reconstruction could be to use the shape of the raw signal, $\mathbf{F}_{\text{sideband}}$, in Figure 4.5. Since the artifacts, and smoothing, originates from the shape of the signal and light configuration, one could decrease the error by compensating for it. For example by suppressing smoothing in the z-direction for Case 1 and reduce large values at the edges of the light-source and detector in Case 2. A combination of the two reconstruction methods could also decrease the error in the image. Since the absorption reconstruction suggests an accurate representation of the tumor but with many artifacts and the ratio reconstruction locate the tumor but does not describe the size of it, a combination of the two methods could put focus on the correct image content, and define the size and shape of the tumor.

Another way to reduce the artifacts would be to use different light configurations since Case 1 and Case 2 resulted in different artifacts. Taking several images with different configurations and averaging these or use tomography could reduce the error. This would however require more images and extended examination sessions.

6 Conclusion

This thesis has investigated how different light configurations can affect the imaging with a UOT-system and techniques to enhance absorption differences from the signal. A larger light-source allows a larger input signal which can increase both the SNR and CNR. The advantage of a rectangular light-source and dividing the detector into two is difficult to interpret since both cases result in artifacts. Ratio and absorption reconstructions have been demonstrated to improve the visibility of absorption changes in the tissue samples in different ways. The ratio reconstruction presented distinct detection of a tumor and the absorption reconstruction included better spatial resolution but more artifacts.

The breast tissue model added complexity to the imaged tissue sample and was one contributing factor to the artifacts in the reconstructions. This emphasized the role of varying scattering in the reconstruction process and the flaws in the reconstruction methods.

References

[1] Hyuna Sung, Jacques Ferlay, Rebecca L. Siegel, Mathieu Laversanne, Isabelle Soerjomataram, Ahmedin Jemal and Freddie Bray. "Global Cancer Statistics 2020: GLOBOCAN Estimates of Incidence and Mortality Worldwide for 36 Cancers in 185 Countries". en. In: *CA: A Cancer Journal for Clinicians* 71.3 (May 2021), pp. 209–249.

[2] Socialstyrelsen. "Screening för bröstcancer - Rekommendation och bedömningsunderlag". sv. In: (2014).

[3] David Hill. "Development of Models, Methods, and Materiel for Deep Tissue Imaging using Light, Ultrasound, and Spectral-Hole Burning". en. PhD thesis. 2023.

[4] Lihong V. Wang and Hsin-i Wu. "Biomedical Optics : principles and imaging". In: Hoboken, New Jersey: John Wiley & Sons, 2007.

[5] Laura A. Sordillo, Yang Pu, Sebastião Pratavieira, Yury Budansky and Robert R. Alfano. "Deep optical imaging of tissue using the second and third near-infrared spectral windows". en. In: *Journal of Biomedical Optics* 19.5 (May 2014), p. 056004.

[6] Scott Prahl. *Optical Absorption of Hemoglobin*. 1999. URL: `https://omlc.org/spectra/hemoglobin/` (visited on 04/10/2022).

[7] L. C. Henyey and J. L. Greenstein. "Diffuse radiation in the Galaxy". en. In: *The Astrophysical Journal* 93 (Jan. 1941), p. 70.

[8] S. A. Prahl. "A Monte Carlo model of light propagation in tissue". en. In: ed. by Gerhard J. Mueller, David H. Sliney and Roy F. Potter. Berlin, Germany, Jan. 1989.

[9] B C Wilson and M S Patterson. "The physics of photodynamic therapy". en. In: *Physics in Medicine and Biology* 31.4 (Apr. 1986), pp. 327–360.

[10] Allan D. Pierce. *Acoustics: An Introduction to Its Physical Principles and Applications*. en. Cham: Springer International Publishing, 2019.

[11] Bahaa E. A. Saleh and Malvin Carl Teich. *Fundamentals of photonics*. 2nd ed. Wiley series in pure and applied optics. Hoboken, N.J: Wiley Interscience, 2007.

[12] Fay A. Marks, Harold W. Tomlinson and Glen W. Brooksby. "Comprehensive approach to breast cancer detection using light: photon localization by ultrasound modulation and tissue characterization by spectral discrimination". en. In: ed. by Britton Chance and Robert R. Alfano. Los Angeles, CA, Sept. 1993, pp. 500–510.

[13] Alexander Bengtsson. “Material and technique development for ultrasound optical tomography using spectral hole burning filters”. PhD thesis. Lund University, 2022.

[14] Y. C. Sun. “Rare Earth Materiais in Optical Storage and Data Processing Applications”. In: *Spectroscopic Properties of Rare Earths in Optical Materials*. Ed. by Robert Hull, Jürgen Parisi, R. M. Osgood, Hans Warlimont, Guokui Liu and Bernard Jacquier. Berlin, Heidelberg: Springer Berlin Heidelberg, 2005, pp. 379–429.

[15] Jord Prangsma. *Noise in detectors for spectroscopy*. 2015. URL: `https://ibsen.com/wp-content/uploads/Tech-Note-Noise-in-linear-array-detectors-v1.0-1.pdf` (visited on 28/11/2022).

[16] Alexander Bengtsson, David Hill, Kevin Shortiss, Lars Rippe and Stefan Kröll. “Comparison of contrast-to-noise ratios of different detection methods in ultrasound optical tomography”. en. In: *Biomedical Optics Express* 13.9 (Sept. 2022), p. 4834.

[17] American National Standard for Safe Use of Lasers. *ANSI Z136.1-2007*. en. Orlando, FL: Laser Institute of America, 2007.

[18] David Hill. *Tagged light simulator*. 2022. URL: `https://bitbucket.org/qilund/tagged-light-simulator/downloads/` (visited on 07/09/2022).

[19] Nicholas Metropolis and S. Ulam. “The Monte Carlo Method”. In: *Journal of the American Statistical Association* 44.247 (1949). Publisher: [American Statistical Association, Taylor & Francis, Ltd.], pp. 335–341.

[20] Lihong Wang, Steven L Jacques and Liqiong Zheng. “MCML - Monte Carlo modeling of light transport in multi-layered tissues”. en. In: *Computer Methods and Programs in Biomedicine* (1995), p. 16.

[21] David Hill, Alexander Bengtsson, Kevin Shortiss, Magnus Cinthio, Jeff Powers, Lars Rippe and Stefan Kröll. “Sequential Monte Carlo Modelling of Ultrasound Optical Tomography: Image Prediction and Absorption Reconstruction in Optically Diffuse Media”. Manuscript in preparation.

[22] T Durduran, R Choe, J P Culver, L Zubkov, M J Holboke, J Giammarco, B Chance and A G Yodh. “Bulk optical properties of healthy female breast tissue”. en. In: *Physics in Medicine and Biology* 47.16 (Aug. 2002), pp. 2847–2861.

[23] Julia L. Sandell and Timothy C. Zhu. “A review of in-vivo optical properties of human tissues and its impact on PDT”. en. In: *Journal of Biophotonics* 4.11-12 (Nov. 2011), pp. 773–787.

[24] R. Graaff, A. C. M. Dassel, M. H. Koelink, F. F. M. de Mul, J. G. Aarnoudse and W. G. Zijlstra. “Optical properties of human dermis in vitro and in vivo”. en. In: *Applied Optics* 32.4 (Feb. 1993), p. 435.

[25] V G Peters, D R Wyman, M S Patterson and G L Frank. “Optical properties of normal and diseased human breast tissues in the visible and near infrared”. en. In: *Physics in Medicine and Biology* 35.9 (Sept. 1990), pp. 1317–1334.

[26] Andreas Walther, Lars Rippe, Lihong V. Wang, Stefan Andersson-Engels and Stefan Kröll. “Analysis of the potential for non-invasive imaging of oxygenation at heart depth, using ultrasound optical tomography (UOT) or photo-acoustic tomography (PAT)”. en. In: *Biomedical Optics Express* 8.10 (Oct. 2017), p. 4523.

[27] Cuiping Li, Nebojsa Duric, Peter Littrup and Lianjie Huang. “In vivo Breast Sound-Speed Imaging with Ultrasound Tomography”. en. In: *Ultrasound in Medicine & Biology* 35.10 (Oct. 2009), pp. 1615–1628.

[28] Kenneth Levenberg. “A method for the solution of certain non-linear problems in least squares”. en. In: *Quarterly of Applied Mathematics* 2.2 (1944), pp. 164–168.

[29] Donald W. Marquardt. “An Algorithm for Least-Squares Estimation of Nonlinear Parameters”. en. In: *Journal of the Society for Industrial and Applied Mathematics* 11.2 (June 1963), pp. 431–441.